Sultam Based Carbonic Anhydrase VII Inhibitors for the Management of Neuropathic Pain

Özlem Akgül [1], Elena Lucarini [2], Lorenzo Di Cesare Mannelli [2], Carla Ghelardini [2], Katia D'Ambrosio [3], Martina Buonanno [3], Simona Maria Monti [3], Giuseppina De Simone [3], Andrea Angeli [4], Claudiu T. Supuran [4] and Fabrizio Carta [4]*

[1] Department of Pharmaceutical Chemistry, Faculty of Pharmacy, Ege University, 35100 Bornova, İzmir-Turkey

[2] NEUROFARBA Department, Section of Pharmacology and Toxicology, Università degli Studi di Firenze, Viale Pieraccini 6, 50139, Florence, Italy.

[3] Institute of Biostructures and Bioimaging, CNR, via Mezzocannone 16, 80134 Naples, Italy.

[4] Università degli Studi di Firenze, NEUROFARBA Dept., Sezione di Scienze Farmaceutiche e Nutraceutiche, Via Ugo Schiff 6, 50019, Sesto Fiorentino (Florence), Italy

*Corresponding Author. E-mail addresses: fabrizio.carta@unifi.it (F.C.)

Abstract. We report a series of compounds **1-17** derived from the antiepileptic drug Sulthiame (**SLT**) from which both the benzenesulfonamide and the sultam moiety were retained. All compounds were tested *in vitro* for their inhibition activity against the human (h) Carbonic Anhydrase (CA; EC 4.2.1.1) I, II, VII, IX and XII isoforms. Among the series, derivatives **1** and **11** showed great enhancement of both inhibition potency and selectivity towards the hCA VII isoform, when compared to the reference **SLT** drug. The binding mode of **11** within the hCA VII active site was deciphered by means of X-ray crystallography and revealed the sultam moiety being exposed to the rim of the active site. *In vivo* experiments on a model of neuropathic pain induced by oxaliplatin clearly showed **11** being an effective pain relieving agent and therefore worth of further exploitation towards the validation of the hCA VII as new target for the management of neuropathies.

Key words: Sultam, Carbonic Anhydrase VII, Neuropathic pain.

1. Introduction

The prominent role of the sultam fragment within fully established drugs and upcoming compounds of experimental use endowed with biomedical features is well documented by a streaming plethora of pioneering scientific reports [1-3]. Such a privileged rank relies on the structural features of the sultam moiety which are all retained from the sulfamide (-SO_2N-) fragment, among which is the stability to hydrolysis when exposed either to extreme pHs or hydrolytic enzymes and its electronic configuration [4]. The latter makes the sulfamide a valid amide bioisostere.

Sultam containing compounds within the field of Carbonic Anhydrase inhibitors (CAIs) for biomedical purposes are well represented among others by the widely used drugs brinzolamide (**BRZ**), sulthiame (**SLT**), trichoromethiazide (**TCM**) or various experimental compounds (**Figure 1**) [5, 6].

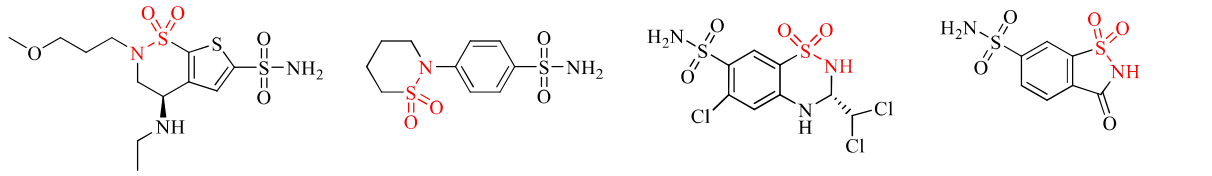

Figure 1. Carbonic Anhydrase Inhibitors comprising the sultam moiety.

In all cases, introduction of the sultam fragment within CAIs by means of diverse molecular rearrangements was primarily intended as a way to make use of the physico/chemical features of a robust moiety. Also such an approach was revealed effective in discriminating among the various human (h) CAs and thus in specifically addressing the biochemical response on the desired isoform with suppression of the side effects derived from nonspecific ligand interactions [7].

Overall, small molecule CAIs for systemic administration still suffer of limited isoform selectivity *in vitro* as result of their compact structure, which physically interacts with a

limited and highly conserved area usually located at the bottom edge of the active site [7]. Molecular elongation brilliantly addresses such an issue by allowing molecular tails to interact with the amino acids placed at the rim of the cavity, which are exclusive for each hCA isoform (i.e. tail approach) [7-12]

The intent of this work is to make use of such an effective approach with the specific intent to obtain CAIs inspired to the antiepileptic **SLT** and endowed with enhanced hCA VII selectivity *in vitro*, and therefore potentially useful for the management of neuropathies associated to the use of platinum-based chemotherapeutic drugs [13]. Indeed, repeated oxaliplatin administrations are well reported to induce a chronic severe dose-limiting neurological syndrome that persists between and after treatments, thus heavily affecting patient's quality of life and in some cases therapeutic compliance [14].

2. Results and Discussion

2.1 Compounds Design and Synthesis

We envisaged to develop our elongation strategy of the antiepileptic **SLT** by means of the fragment based drug design (FBDD) approach and assuming as growing vector the distal end of the molecule facing towards the catalytic site rim [15, 16]. From the chemical view point we considered either: *i*) to preserve the **SLT** molecular fragments which allow such compound to act as good inhibitor of the hCA VII (i.e. the benzenesulfonamide and the sultam ring) [17]; *ii*) to split them apart and to insert a flexible tether in between. Such a design strategy perfectly fits with compounds of the type in **Figure 2** recently reported by some of us [18]. For the purposes of this study the taurultam moiety resulted ideal as it arranged, in agreement to the indicated FBDD growing vector, the sultam key fragment with a tertiary amine worth of establishing additional hydrogen bond interactions with the enzymatic

target and of easy derivatization and thus giving access to the chemical diversity necessary for our explorations (**Figure 2**).

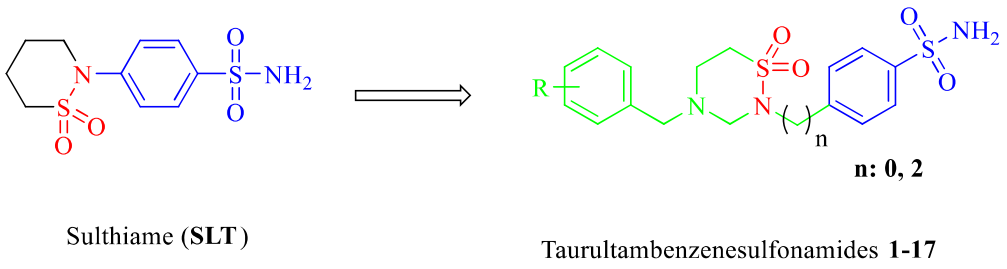

Figure 2. Schematic representation of the drug design strategy

Briefly, the compounds **1-17** here considered were synthesized in agreement with the procedures reported by some of us and characterized by means of 1H NMR and 13C NMR [18]. Obtained compounds resulted ≥ 95% purity by high-resolution mass spectrometry (HRMS) analysis (**Supporting Information**).

2.2 Carbonic Anhydrase Inhibition

All the newly prepared compounds **1-17** were screened for their inhibition efficacy against the five physiologically relevant isoforms hCA I, II, VII, IX and XII by means of the stopped-flow CO_2 hydrase assay [19]. These data were compared to those previously obtained for acetazolamide (**AAZ**), **SLT** [17], saccharine-6-sulfonamide (**SCC**) [8] and **TCM** [20] as reference drugs (**Table 1**).

Table 1 Stopped-flow kinetic data of compounds **1–17** on hCAs I, II, VII, IX and XII in comparison with **AAZ**, **SLT**, **SCC** and **TCM**.

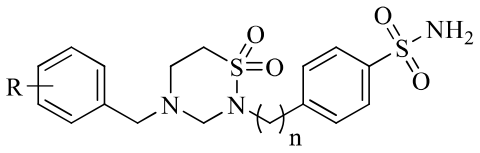

1-17 **1-9 n=0**
10-17 n=2

		K_I (nM)*				
	R	**CA I**	**CA II**	**CA VII**	**CA IX**	**CA XII**
1	-H	4652	210.4	8.7	1141	285.2
2	4-methyl	5430	84.5	27.2	176.7	520.9
3	4-fluoro	941.7	218.7	22.5	1317	744.4
4	4-trifluoromethyl	7641	40.1	34.2	290.2	71.3
5	4-nitro	7863	242.2	83.1	2659	773.6
6	4-isopropyl	4207	96.8	257.6	310.1	767.3
7	perfluoro	2441	89.6	8.9	969.3	97.6
8	4-metoxy	4489	87.8	588.1	186.2	78.5
9	3-chloro	3410	82.1	45.2	317.3	359.5
10	-H	763.5	30.5	34.7	822.8	632.8
11	4-methyl	629.1	51.5	2.5	1842	213.8
12	4-fluoro	1905	86.7	73.2	2146	8.9
13	4-trifluoromethyl	647.8	37.2	57	1791	574.5
14	4-nitro	4413	26.9	55	297.5	52.8
15	4-tert-butyl	7740	216.6	30.2	1206	9.6
16	2,4-difluoro	5378	56.5	85.5	1664	9.7
17	4-chloro	2054	42.8	6.8	2270	8.6
AAZ		250	12.1	2.5	25.8	5.7
SLT [17]		374	7.0	6.0	43.0	56.0
SCC [8]		3406	77.3	6.7	113	64.8
TCM [20]		345	91	7.9	87	312

*Mean from 3 different assays by a stopped-flow technique (errors were in the range of ± 5–10% of the reported values)

Overall inspection of the data in **Table 1** accounted for the shortest derivatives **1-9** being preferential inhibitors for the central nervous system (CNS) abundantly expressed hCA VII isoform with K_I values falling within the medium-low nanomolar range. As for the longer compounds **10-17** such a kinetic profile was mislaid in favor of the tumor associated hCA XII. Deeper structure-activity relationships (SARs) for the two series are below discussed:

i) The hCA I isoform resulted inhibited in micromolar concentrations from compounds **1-17** that therefore resulted far less efficient when compared to the reference drug **AAZ** (i.e. K_I 250 nM). Among the sulfanilamide series **1-9** it is worth noting the 4.9-fold potency increase after introduction of the fluorine atom in **1** to afford the derivative **3** (K_Is of 4652 and 941.7 nM, respectively), which is the most potent hCA I inhibitor among the series. The introduction of various moieties within the benzyl scaffold in the remaining derivatives did not allow to extrapolate any rational outcome. Molecular elongation with the ethyl spacer as in **10-17**, radically changed the kinetic profile as revealed when shorter compounds sharing the same benzyl tail are compared. For instance the introduction in **10** of the methyl, fluoro and trifluoromethyl groups at position 4 of the benzyl tail (i.e. compounds **11-13**) resulted in opposite effects on the hCA I isoform, when compared to their shorter analogues **2-4**. The only exception was represented by the nitro moiety which in both series (i.e. compounds **5** and **14**) weakened the inhibition potency for the hCA I. As for the remaining compounds **15-17** no SAR considerations are counted as an increase of the K_I values is observed regardless of the electronic and/or bulkiness of the moiety introduced (see **Table 1**).

ii) The catalytic efficient and housekeeping hCA II isoform resulted more sensitive to the compounds considered in this study. Among the shortest series, only the 4-fluoro and 4-nitro derivatives **3** and **5** showed higher K_I values when compared to the progenitor benzyl derivative **1** (see **Table 1**). It is worth speculating that such an effect is associated to the mere electron-withdrawing nature of both the halogen and the nitro moieties as proven by a considerable reduction of the hCA II K_I value when the highly hydrophobic, electron-rich and sterically demanding trifluoromethyl moiety, as in compound **4,** was instead introduced [21, 22]. Interestingly, the compound **4** resulted the most potent hCA II inhibitor among the sulfanilamide containing series **1-9** (K_I of 40.1 nM). As for the remaining ones (i.e. **2**, **6-9**) an almost flat kinetic profile was reported with no relevant SAR considerations to report (see **Table 1**). Again molecular elongation by means of the ethylenic spacer as in **10-17** determined a complete change of the kinetic outcome. Replacement of the benzyl tail in **10** with the 4-methyl and 4-fluorobenzyl ones, to afford **11** and **12**, spoiled the hCA II inhibition potencies up to 2.84-fold (K_Is of 30.5, 51.5 and 86.7 nM, respectively). Interestingly the 4-trifluoromethyl and the 4-nitro derivatives **13** and **14** restored the K_I inhibition values to the low nanomolar range with the latter being the most potent hCA II inhibitor among the entire series (K_Is of 37.2 and 26.9 nM respectively). On the contrary the introduction of the 2,4-difluoro and 4-chloro moieties determined significative enhancement of the associated K_I values (see **Table 1**).

iii) Overall, the compound series **1-17** was very effective in inhibiting the abundantly CNS expressed hCA VII with the majority of K_I values being in the low nanomolar range (**Table 1**). Among the shortest derivatives **1-9**, the unsubstituted benzyl compound **1** was the most potent in inhibiting the hCA VII isoform, with a K_I of 8.7 nM and thus just 3.5-fold less potent when compared to the reference **AAZ** (K_I of 2.5 nM). Interestingly, the perfluoro benzyl substituted derivative **7** showed a close matching K_I value to **1** (see **Table**

1). Both the 4-methyl and 4-fluoro insertion on the molecular tail resulted in similar inhibition effects (K_Is of 27.2 and 22.5 nM for **2** and **3,** respectively), which were further spoiled when the 4-trifluoromethyl, the 3-chloro and the 4-nitro moieties were considered instead (K_Is of 34.2, 45.2 and 83.1 nM for **4**, **9** and **5,** respectively). Significative reduction of the hCA VII inhibition potency was observed when the bulky 4-isopropyl group was inserted (compound **6**). More importantly it is worth noting the great effect on kinetics when the methyl group in compound **2** was substituted with the methoxy in **8**, as the latter showed a K_I value 21.6-fold higher when compared to the former (**Table 1**). As for the longer series **10-17** the kinetic outcome on the hCA VII resulted far less consistent and far more difficult to rationalize when compared to the shortest counterparts **1-9** (**Table 1**). For instance the unsubstituted benzyl **10** showed an inhibition potency slightly higher than the bulky 4-tert-butyl derivative **15** (K_Is of 34.7 and 30.2 nM, respectively). The introduction of the 4-methyl group greatly enhanced the inhibition potency which was as much as the reference **AAZ** (K_Is of 2.5 nM). Single or double insertion within **10** of fluorine atoms, as in **12** and **16**, spoiled the inhibition potency up to 2.5-fold. Finally the pure electron-withdrawing nitro moiety in **14** determined inhibition potency against the hCA VII as much as the hydrophobic, electron-rich and bulky trifluoromethyl group placed at the same position in compound **13** (K_Is of 55 and 57 nM, respectively).

iv) The tumor associated hCA IX isoform was the least inhibited from the compounds considered in this study, being the 4-methyl and the 4-methoxy derivatives (i.e. **2** and **8**) the most potent inhibitors among all with K_I values of 176.7 and 186.2 nM respectively. As for the remaining derivatives, inhibition values between the high nanomolar-low micromolar range were observed with a rather confusion SAR correlation. On the contrary, hCA XII showed a quite interesting inhibition profile. Among the sulfanilamides **1-9**, the 4-trifluoromethyl and the 4-methoxy benzyl derivatives resulted the most effective

inhibitors with K_Is of 71.3 and 78.5 nM, respectively. Also in this case it is worth highlighting the huge impact on the inhibition potency when the 4-methoxy in compound **8** was replaced with a 4-methyl as in **2** since a 6.2-fold decrease was observed (K_Is of 78.5 and 520.9 nM respectively). Of particular interest are the longer derivatives **10-17**. The introduction of the 4-methyl moiety in **1** determined a 3-fold potency increase against hCA XII (K_Is of 213.8 for compound **11**). Moreover, insertion of the fluorine atom at the same position, as in compound **12**, further enhanced the inhibition potency up to 24-fold (K_I of 8.9 for **12**). Such a value was only slightly higher when compared to the reference **AAZ** of 5.7 nM and it was also reported for the 3-chloro derivative **17** (K_I of 8.6 nM). Although the 2,4-fluoro substitution retained the strong inhibition for the hCA XII isoform (i.e. K_I 9.7 nM), it is peculiar that the 4-*tert*-butyl group, which is electronically and sterically diverse from the halogen, shows an almost matching K_I of 9.6 nM.

Among the compounds profiled within this study the high selectivity of compounds **1** and **11** for the CNS abundantly expressed hCA VII, as demonstrated in **Table 2**, is far superior to known structurally related drugs, such as **SLT,** which is currently used in clinics for the management of epilepsy, the diuretic **TCM** or the experimental compound **SCC** (**Table 2**).

Table 2. Selectivity indexes (SIs) of compound **1**, **11**, **SLT**, **SCC** and **TCM** for the hCA VII over the hCA II, IX and XII isoforms.

	SI (K_I hCA*n*/K_I hCA VII)		
	II/VII	**IX/VII**	**XII/VII**
1	24.2	131.1	32.8
11	20.4	736.8	85.2
SLT	1.2	7.2	9.3
SCC	11.5	16.9	9.7
TCM	11.5	11.0	39.5

All the inhibition data clearly sustained the success of our elongation strategy on the **SLT**, thus obtaining derivatives far more effective and selective inhibitors for hCA VII.

2.3 X-Ray crystallography

In consideration of the kinetic profile reported for compound **11**, we decided to deeply investigate it by means of X-ray crystallography, in order to identify the structural reasons underpinning its selectivity. Crystals of the hCA VII/**11** adduct were obtained using the soaking technique as previously reported [11], whereas data collection and refinement were performed as reported in the experimental section (**Table S2**).

Electron density maps (|Fo-Fc| and |2Fo-Fc| maps), calculated at various stages of the crystallographic refinement, clearly showed the presence of one inhibitor entirely allocated within the active site cavity (**Figure S1**). Of interest is the tail of the molecule which was flipped inwards the enzyme cleft and connected to the sultam group exposed to the rim cavity (**Figure 3**). As already reported for CAIs of the benzenesulfonamide type [9], compound **11** was anchored to the enzyme through the sulfonamide moiety which coordinated the Zn^{2+} ion in the ionized NH^{-} form and established hydrogen bond interactions with the conserved T199 residue (**Figure 3**). The phenyl ring was located in the middle of the active site and was engaged in strong (<4.0 Å) van der Waals contacts with His94, Val121, Leu198 and Thr200. The ethyl-taurultam linker established van der Waals contacts with residues Phe131, Gly132, Ala135 and Pro202, whereas the toluene moiety interacts with Trp5, Asn62, His64, Thr200 and Pro201 (**Figure 3**).

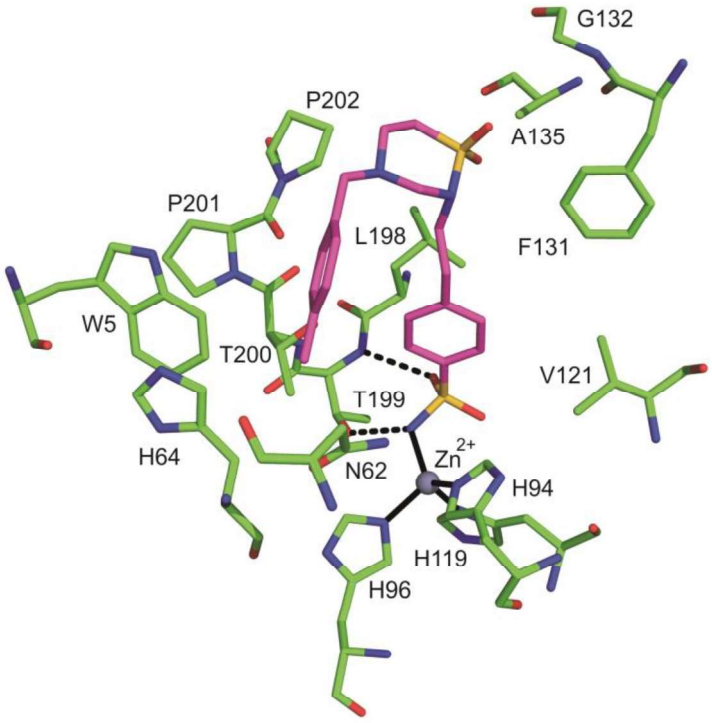

Figure 3. Active site region of the hCA VII/**11** adduct. The zinc ion coordination (continuous lines), hydrogen bonds (dashed lines) and protein residues involved into van der Waals interactions with the inhibitor are shown.

Comparison of hCA VII/**11** with the hCA II isoform in adduct with **SLT** (PDB 2Q1Q) [17], **SCC** (PDB 4XE1) [8] and **TCM** (PDB 1ZGF) [23] allowed to identify the molecular determinants responsible for the different selectivity of these compounds toward the diverse hCAs (**Figure 4**). All these inhibitors coordinate the catalytic Zn^{2+} ion by means of the primary sulfonamide whereas the secondary sulfonamide of the sultam fragment interacts with amino acid residues defining the enzymatic site [17, 8, 23]. In particular, such a group both in **SCC** and **TCM**, where it is condensed with the benzenesulfonamide ring, is placed in the middle-high region of the hCA II cavity, with the secondary sulfonamide being oriented respectively towards the hydrophobic and hydrophilic region of the site (**Figure 4A**) [8, 23]. In the hCA II/**SLT** adduct, the sultam fragment, which is structurally connected and thus not

merged to the benzensulfonamide, still interacts with the hydrophilic region of the cleft although resulting slightly lifted up towards the rim of the cavity [14], when compared to both hCA II/**SCC** and hCA II/**TCM** adducts (**Figure 4B**). Finally, in the complex under investigation, the presence of the ethyl linker permits the taurultam ring to further drive up within the cavity reaching the protein surface and interacting with residues which delimit the rim of the active site, which is the most variable region among the different human isoforms [9-11] (**Figure 4C** and **Table 3**).

These crystallographic data validate our FBDD growing vector approach as shifting the valuable sultam fragment towards the top edge of the catalytic cleft and in the correct orientation greatly increases the selectivity of the ligand (**Table 1** and **2**).

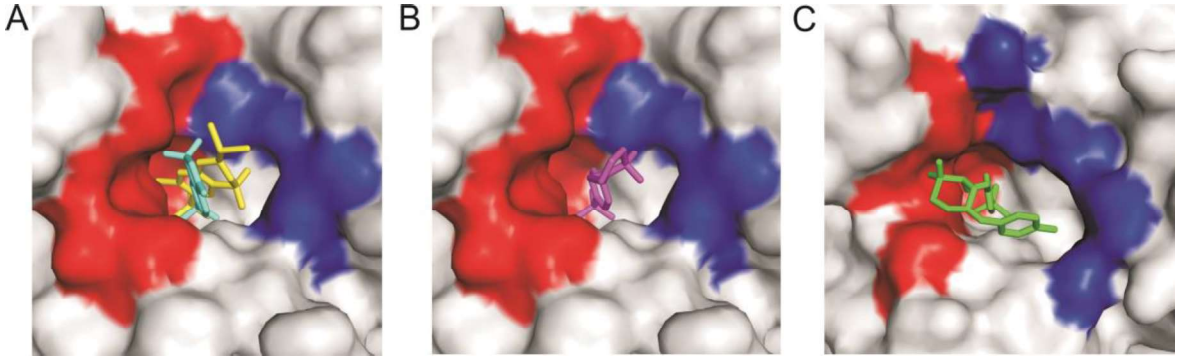

Figure 4. (**A**) Superposition of inhibitors **TCM** (yellow) (PDB code 1ZGF) and **SCC** (cyan) (PDB code 4XE1) bound to the hCA II active site; (**B**) hCA II/**SLT** (PDB code 2Q1Q); (**C**) hCA VII/**11**. The enzymes are represented as a surface-model (hydrophobic region of the active site in red, hydrophilic region in blue).

Table 3. hCA VII residues interacting with the different fragments of compound **11**. The corresponding residues in isoforms I, II, IX and XII are shown. Not conserved residues are shown in red.

	CA VII	**CA I**	**CA II**	**CA IX**	**CA XII**
Benzenesulfonamide					
	H94	H	H	H	H

	V121	A	V	V	V
	L198	L	L	L	L
	T200	H	T	T	T
Ethyl-taurultam					
	F131	L	F	V	A
	G132	A	G	D	S
	A135	A	V	L	S
	P202	P	P	P	P
Toluene					
	W5	W	W	Q	W
	N62	V	N	N	N
	H64	H	H	H	H
	T200	H	T	T	T
	P201	P	P	P	P

2.4 *In vivo* efficacy of hCA VII inhibitors in relieving the chemotherapy-induced neuropathic pain.

Selected compounds **1**, **2** and **11** were evaluated *in vivo* for their ability in relieving the neuropathic pain induced by the anticancer drug oxaliplatin and compared to the effects achieved with duloxetine, the standard drug clinically used for the management of chemotherapy-induced neuropathy (**Figure 5**) [24, 25].

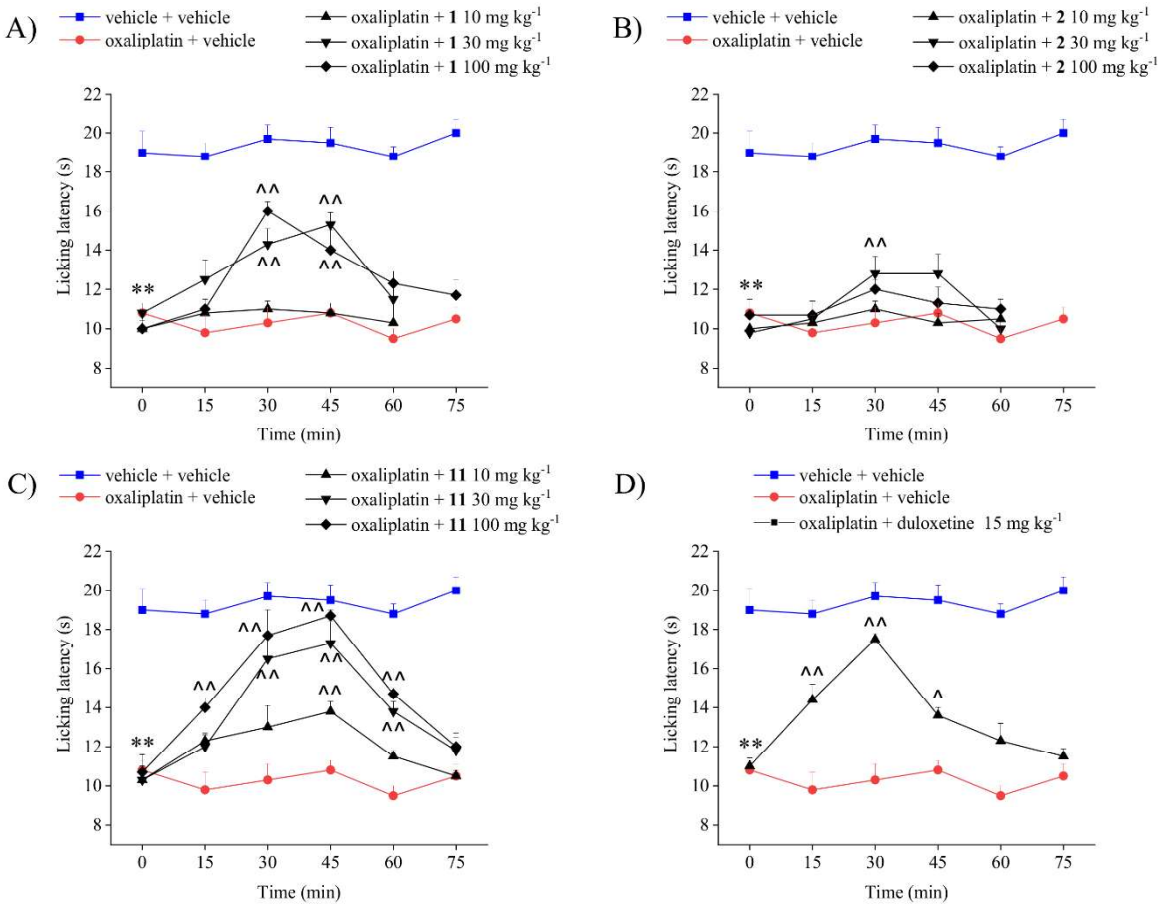

Figure 5. (**A–D**) Effects of acute administration of CAIs **1, 2, 11** and duloxetine on oxaliplatin-induced neuropathic pain in the mouse measured by the cold plate test. Oxaliplatin (2.4 mg kg^{-1}) was intraperitoneal (i.p.) administered for 5 consecutive days every week for 2 weeks and showed a licking latency to 10.8 ± 0.5 s in comparison to 19.0 ± 1.1 s of the control group (vehicle + vehicle group). Compounds were dissolved in 1% carboxymethylcellulose sodium salt (CMC) and administered per o.s. acutely when neuropathy was well established (day 15). Each value represents the means ± SEM of 10 mice collected in two different experimental sets. Statistical analysis is one-way ANOVA followed by Bonferroni's post-hoc comparison. $^{**}P < 0.01$ vs vehicle + vehicle-treated animal; $^{\wedge}P < 0.05$ and $^{\wedge\wedge}P < 0.01$ vs oxaliplatin + vehicle-treated animals.

Compound **1** resulted partially effective in relieving the neuropathic pain induced by oxaliplatin injection. Either the dose of 30 or 100 mg kg^{-1} was able to significantly increase animals pain threshold 30-45 min after the injection, although without reaching the value of controls (vehicle + vehicle group; **Figure 5A**). By contrast, compound **2** was almost ineffective with a slight increase of the pain threshold 30 min after administration at the maximum dosage of 100 mg kg^{-1} (**Figure 5B**). The best antinociceptive profile was obtained with compound **11**. In particular, the doses of 30 and 100 mg kg^{-1} were able to significantly increase the animals licking latency up to 60 min after treatment with a peak of efficacy placed between 30 and 45 minutes. At these times, the animals receiving compound **11** at 100 mg kg^{-1} displayed a pain threshold near to that of controls (vehicle + vehicle group; **Figure 5C**). Noteworthy the pain-relieving efficacy of the compound **11** resulted comparable (at 30 mg kg^{-1}) or even greater (at 100 mg kg^{-1}) than that induced by duloxetine (15 mg kg^{-1}), which picked at 30 min and lasted up to 45 min (**Figures 5C** and **D**). Despite the encouraging results obtained with compound **11** and the nearly matching effects with duloxetine at half the concentration, it is appropriate to consider that the associated pharmacological mechanisms are different and not related [26]. Compounds 1, 2 and 11 did not induce behavioral alterations attributable to toxic effect; furthermore the dose 3 fold higher of that tested during pain threshold analysis (300 mg kg -1) did not induced significant change of neurobehavioral physiological parameters as evaluated by the Irwin test (**Table S3**). Such consideration further sustains the hCA VII as alternative/adjunctive target for the management of neuropathic pain.

3. Conclusions

Herein we successfully reported an efficient strategy applied to the antiepileptic drug **SLT**, which resulted in the obtainment of compounds **1** and **11** endowed with enhanced affinity and selectivity for the CNS abundantly expressed hCA VII over the other isoforms considered.

The binding mode of **11** in adduct with the hCA VII isoform was investigated by means of X-ray crystallography and revealed that the sultam moiety was exposed to the rim of the active site, which is the most variable region among the different CA isoforms, with the distal tolyl flipped back into the enzymatic cavity. In addition the derivative **11** revealed being an effective relieving agent when tested *in vivo* against oxaliplatin induced neuropathic pain with effects comparable to the reference drug duloxetine. Overall the data obtained in this study laid a first line of knowledge useful for further development of hCA VII inhibitors based on key fragments identified on drugs actually used in clinic. Moreover the *in vivo* results give solid evidences for the validation of the hCA VII as alternative/adjunctive target useful for the management of persistent pain with particular emphasis that associated to the use of platinum based chemotherapeutic drugs.

4. Experimental section

4.1. Chemistry

Compounds **1-17** studied here were synthesized, purified and characterized according to our previous report [18]. All final compounds were obtained in good yields and with high-purity grade (≥95%) as determined on Agilent Technologies 6530 Accurate-Mass Q-TOF LC/MS. [18]. Chemical structures and synthesis are reported in the Supporting Information (**Table S1**).

4.2 CA Inhibition

An Applied Photophysics stopped-flow instrument was used for assaying the CA catalyzed CO_2 hydration activity [19]. Phenol red (at a concentration of 0.2 mM) was used as an indicator, working at the absorbance maximum of 557 nm, with 20 mM Hepes (pH 7.4) as buffer and 20 mM Na_2SO_4 for maintaining constant ionic strength, following the initial rates of the CA-catalyzed CO_2 hydration reaction for a period of 10–100 s. The CO_2 concentrations ranged from 1.7 to 17 mM for the determination of the kinetic parameters and inhibition

constants. For each inhibitor, at least six traces of the initial 5–10% of the reaction were used for determining the initial velocity. The uncatalyzed rates were determined in the same manner and subtracted from the total observed rates. Stock solutions of the inhibitor (0.1 mM) were prepared in distilled–deionized water and dilutions up to 0.01 nM were done thereafter with the assay buffer. Inhibitor and enzyme solutions were preincubated together for 15 min at room temperature prior to the assay, to allow for the formation of the E–I complex. The inhibition constants were obtained by non-linear least-squares methods using PRISM 3 and the Cheng-Prusoff equation as reported earlier and represent the mean from at least three different determinations. All CA isoforms were recombinant proteins obtained inhouse, as reported earlier [19, 27-29].

4.3 X-Ray crystallography

Home-made hCA VII was obtained following an experimental procedure previously reported [30]. A mutated form of the enzyme where the cysteine residues in position 183 and 217 were mutated into serines was used, since this mutant is more suitable for crystallization [30]. Crystals of the hCA VII/**11** complex were obtained by using the soaking technique. In particular, crystallization experiments on hCA VII were performed by the hanging-drop vapor-diffusion method at 20 °C. Drops were prepared mixing equivalent volumes of protein (5 mg/mL in 0.02 M, Tris-HCl pH 8.0 and 0.1 M NaCl) and precipitant solution (17% v/v Peg 3350, 0.2 M Ammonium acetate and 0.1 M Tris pH 8.5) and then equilibrated against 1 mL of precipitant solution. Crystals grew in a couple of days and some of them were transferred in a 2 μL drop, containing the precipitant solution, the inhibitor at a concentration of 6 mM and 25% glycerol (w/v). These crystals were kept in the soaking solution for 6 hours and then flash-frozen in a gas nitrogen stream. X-ray diffraction data were collected at the Elettra Synchrotron Light Source (Trieste) by using one single crystal. Diffraction data were

collected at Elettra Synchrotron Light Source (Trieste) (wavelength 1.0 Å, beam size 100 μm, crystal-to-detector distance 236.38 mm, at 100 K) by using one single crystal. Data were collected using the oscillation method in intervals of 0.5° steps on a Pilatus 6M detector (Dectris). A total of 720 images were collected. Diffraction data were indexed, integrated and scaled using the HKL2000 software package [31]. Initial phases were calculated using the atomic coordinates of the unbound hCA VII (PDB accession code 6G4T) with waters removed [30]. The structure was refined using the CNS program [32], whereas model building and map inspections were performed using the O program [33]. In particular, an initial round of rigid body refinement was followed by simulated annealing and isotropic thermal factor (B-factor) refinement. The inspection of electron density maps, at various stages of crystallographic refinement, clearly showed the binding of one inhibitor molecule in the active site cavity (**Figure S1**). These maps were well defined for the benzenesulfonamide moiety and the ethyl-taurultam linker of the inhibitor, while a poorer definition was observed for the toluene group. Restraints on inhibitor bond angles and distances were taken from similar structures in the Cambridge Structural Database [34] and standard restraints were utilized on protein bond angles and distances during refinement [35]. The ordered water molecules were added automatically and checked individually. Each peak contoured at 3σ in the |Fo - Fc| maps was identified as a water molecule, assuring that hydrogen bonds would be allowed between this site and the model. Several alternating cycles of energy minimization, individual temperature factor refinement and manual model building gave the final model with R-work/R-free values of 0.189 and 0.206. Topology files for inhibitor **11** were obtained using the Xplor2d server [36]. The stereochemical quality of the model was finally checked using Procheck [37] and Whatcheck [38] programs. Refinement statistics are reported in **Table S1**.

4.4 Biological Studies

4.4.1 Animals

Male CD-1 albino mice (Envigo, Varese, Italy) weighing approximately 22–25 g at the beginning of the experimental procedure were used. Animals were housed in Ce.S.A.L (Centro Stabulazione Animali da Laboratorio, University of Florence) and used at least 1 week after their arrival. Ten mice were housed per cage (size 26 × 41 cm); animals were fed a standard laboratory diet and tap water *ad libitum* and kept at 23 ± 1 °C with a 12 h light/dark cycle, light at 7 a.m. All animal manipulations were carried out according to the Directive 2010/63/EU of the European Parliament and of the European Union Council (22 September 2010) on the protection of animals used for scientific purposes. The ethical policy of the University of Florence complies with the Guide for the Care and Use of Laboratory Animals of the US National Institutes of Health (NIH publication no. 85-23, revised 1996; University of Florence assurance number: A5278-01). Formal approval to conduct the experiments described was obtained from the Animal Subjects Review Board of the University of Florence. Experiments involving animals have been reported according to ARRIVE guidelines [39]. All efforts were made to minimize animal suffering and to reduce the number of animals used.

4.4.2 Chemotherapy-induced neuropathic pain model and pharmacological treatments

Chemotherapy-induced neuropathy was induced in mice by i.p. administration of oxaliplatin (2.4 mg kg^{-1}) on days 1-2, 5–9, and 12–14 (10 i.p. injections) [40, 41]. Oxaliplatin was dissolved in 5% glucose solution. Control animals received an equivalent volume of vehicle. Behavioral tests were performed starting from day 15. Duloxetine (15 mg kg^{-1}), compounds **1**, **2** and **11** (10–100 mg kg^{-1}) were suspended in 1% carboxymethylcellulose sodium salt

(CMC, Sigma-Aldrich, Milan, Italy) and per os (p.o.) acutely administered. Behavioral tests were carried out before and after (15, 30, 45, 60 and 75 min) compound's injection.

4.4.3 Cold plate test

Thermal allodynia was assessed using the cold plate test. With minimal animal–handler interaction, mice were taken from home cages and placed onto the surface of the cold plate (Ugo Basile, Varese, Italy) maintained at a constant temperature of 4 °C ± 1 °C. Ambulation was restricted by a cylindrical Plexiglas chamber (diameter: 10 cm; height: 15 cm), with an open top. A timer controlled by foot pedal began timing response latency from the moment the mouse was placed onto the cold plate. Pain-related behaviour (licking of the hind paw) was observed, and the time (seconds) of the first sign was recorded. The cut-off time of the latency of paw lifting or licking was set at 30 s [42].

4.4.4 Statistical analysis

Behavioral measurements were performed on 10 mice for each treatment carried out in two different experimental sets. Results were expressed as means ± SEM. The analysis of variance of behavioral data was performed by one-way ANOVA, and a Bonferroni's significant difference procedure was used for post-hoc comparison. *P* values of less than 0.05 or 0.01 were considered significant. Investigators were blind to all experimental procedures. Data were analyzed using the "Origin 9" software (OriginLab, Northampton, USA).

ASSOCIATED CONTENT

The Supporting Information is available free of charge at https://XXX. Complete list of the analyzed compounds **1-17** (**Table S1**) and synthetic procedures; Electron density maps of compound **11** bound withi hCA VII (**Figure S1**); Data collection and refinement statistics for hCA VII/**11** complex (**Table S2**); Irwin test (**Table S3**); Irwin test methodology. Coordinates and structure factors have been deposited in the Protein Data Bank (accession code **7P1A**) and will be released upon acceptance of the manuscript.

AUTHOR INFORMATION

Corresponding author

Dr. Fabrizio Carta (F.C.). NEUROFARBA Department, Sezione di Scienze Farmaceutiche e Nutraceutiche, Università degli Studi di Firenze, 50019 Sesto Fiorentino (Florence), Italy; E-mail address: fabrizio.carta@unifi.it

Authors

Özlem Akgül. Department of Pharmaceutical Chemistry, Faculty of Pharmacy, Ege University, 35100 Bornova, İzmir-Turkey

Elena Lucarini. NEUROFARBA Department, Section of Pharmacology and Toxicology, Università degli Studi di Firenze, Viale Pieraccini 6, 50139, Florence, Italy.

Lorenzo Di Cesare Mannelli. NEUROFARBA Department, Section of Pharmacology and Toxicology, Università degli Studi di Firenze, Viale Pieraccini 6, 50139, Florence, Italy.

Carla Ghelardini. NEUROFARBA Department, Section of Pharmacology and Toxicology, Università degli Studi di Firenze, Viale Pieraccini 6, 50139, Florence, Italy.

Katia D'Ambrosio. Institute of Biostructures and Bioimaging, CNR, via Mezzocannone 16, 80134 Naples, Italy.

Martina Buonanno. Institute of Biostructures and Bioimaging, CNR, via Mezzocannone 16, 80134 Naples, Italy.

Simona Maria Monti. Institute of Biostructures and Bioimaging, CNR, via Mezzocannone 16, 80134 Naples, Italy.

Giuseppina De Simone. Institute of Biostructures and Bioimaging, CNR, via Mezzocannone 16, 80134 Naples, Italy.

Andrea Angeli. Università degli Studi di Firenze, NEUROFARBA Dept., Sezione di Scienze Farmaceutiche e Nutraceutiche, Via Ugo Schiff 6, 50019, Sesto Fiorentino (Florence), Italy

Claudiu T. Supuran. Università degli Studi di Firenze, NEUROFARBA Dept., Sezione di Scienze Farmaceutiche e Nutraceutiche, Via Ugo Schiff 6, 50019, Sesto Fiorentino (Florence), Italy

Author Contributions

The manuscript was written through contributions of all authors. All authors have given approval to the final version of the manuscript.

Acknowledgments.

Ozlem Akgul (O.A.) is grateful to The Scientific and Technical Research Council of Turkey [TUBİTAK 117S516] and Ege University [16-ECZ-012].

Fabrizio Carta (F.C.) is grateful to "Bando di Ateneo per il Finanziamento di Progetti Competitivi per Ricercatori a Tempo Determinato (RTD) dell'Università di Firenze - 2020-2021" and Fondazione Cassa di Risparmio di Firenze (Grant Number ECR2018.1001) which partially funded this work.

Abbreviations

CA, carbonic anhydrase; CAI(s), carbonic anhydrase inhibitor(s); AAZ, acetazolamide; SLT, Sulthiame;

Declaration of Competing Interest

The authors declare that they have no known competing financial interests or personal relationships that could have appeared to influence the work reported in this paper.

References

[1] K.C. Majumdar, S. Mondal, Recent Developments in the Synthesis of Fused Sultams. *Chem. Rev*. 111 (2011) 7749–7773. https://doi.org/10.1021/cr1003776.

[2] P.M. Okwuchukwu, D. Bandyopadhyay, Medicinally Privileged Sultams: Synthesis and Mechanism of Action. *Mini-Reviews Med. Chem*. 20 (2021) 2193–2206. https://doi.org/10.2174/1389557520666200719015234.

[3] C. Zhao, K.P. Rakesh, L. Ravidar, W.Y. Fang, H.L. Qin, Pharmaceutical and medicinal significance of sulfur (SVI)-Containing motifs for drug discovery: A critical review. *Eur. J. Med. Chem*. 162 (2019) 679–734. https://doi.org/10.1016/j.ejmech.2018.11.017.

[4] S. Senger, C. Chan, M.A. Convery, J.A. Hubbard, G.P. Shah, N.S. Watson, R.J. Young, Sulfonamide-related conformational effects and their importance in structure-based design. *Bioorg. Med. Chem. Lett*. 17 (2007) 2931–2934. https://doi.org/10.1016/j.bmcl.2007.02.034.

[5] D.A. Adsmond, D.J.W. Grant, Hydrogen bonding in sulfonamides. *J. Pharm. Sci.* 90 (2001) 2058–2077. https://doi.org/10.1002/jps.1157.

[6] J.M. Langenhan, J.D. Fisk, S.H. Gellman, Evaluation of hydrogen bonding complementarity between a secondary sulfonamide and an α-amino acid residue. *Org. Lett*. 3 (2001) 2559–2562. https://doi.org/10.1021/ol016237x.

[7] K. D'Ambrosio, F.-Z. Smaine, F. Carta, G. De Simone, J.-Y. Winum, C.T. Supuran, Development of Potent Carbonic Anhydrase Inhibitors Incorporating Both Sulfonamide and Sulfamide Groups. *J. Med. Chem*. 55 (2012) 6776–6783. https://doi.org/10.1021/jm300818k.

[8] V. Alterio, M. Tanc, J. Ivanova, R. Zalubovskis, I. Vozny, S.M. Monti, A. Di Fiore, G. De Simone, C.T. Supuran, X-ray crystallographic and kinetic investigations of 6-

sulfamoyl-saccharin as a carbonic anhydrase inhibitor. *Org. Biomol. Chem*. 13 (2015) 4064–4069. https://doi.org/10.1039/C4OB02648A.

[9] V. Alterio, A. Di Fiore, K. D'Ambrosio, C.T. Supuran, G. De Simone, Multiple Binding Modes of Inhibitors to Carbonic Anhydrases: How to Design Specific Drugs Targeting 15 Different Isoforms?. *Chem. Rev*. 112 (2012) 4421–4468. https://doi.org/10.1021/cr200176r.

[10] V. Alterio, M. Hilvo, A. Di Fiore, C. T. Supuran, P. Pan, S. Parkkila, A. Scaloni, J. Pastorek, S. Pastorekova, C. Pedone, A. Scozzafava, S. M. Monti, G. De Simone. Crystal structure of the catalytic domain of the tumor-associated human carbonic anhydrase IX. *Proc. Natl. Acad. Sci. U. S. A.* 106 (2009) 16233-16238. doi: 10.1073/pnas.0908301106.

[11] K. D'Ambrosio, A. Di Fiore, M. Buonanno, S. Kumari, M. Tiwari, C. T. Supuran, C. B. Mishra, S. M. Monti, G. De Simone. The crystal structures of 2-(4-benzhydrylpiperazin-1-yl)-N-(4-sulfamoylphenyl)acetamide in complex with human carbonic anhydrase II and VII provide insights into selective CA inhibitor development. *New J. Chem.* (45) 2021 147-152 doi: 10.1039/D0NJ03544K

[12] C.T. Supuran, Emerging role of carbonic anhydrase inhibitors. *Clin. Sci*. 135 (2021) 1233–1249. https://doi.org/10.1042/CS20210040.

[13] N.P. Staff, A. Grisold, W. Grisold, A.J. Windebank, Chemotherapy-induced peripheral neuropathy: A current review. *Ann. Neurol.* 81 (2017) 772–781. https://doi.org/10.1002/ana.24951.

[14] A.J.M. Beijers, F. Mols, G. Vreugdenhil, A systematic review on chronic oxaliplatin-induced peripheral neuropathy and the relation with oxaliplatin administration, *Support. Care Cancer.* 22 (2014) 1999–2007. https://doi.org/10.1007/s00520-014-2242-z.

[15] J.D. St. Denis, R.J. Hall, C.W. Murray, T.D. Heightman, D.C. Rees, Fragment-based drug discovery: opportunities for organic synthesis. *RSC Med. Chem*. 12 (2021) 321–329. https://doi.org/10.1039/D0MD00375A.

[16] C.W. Murray, D.C. Rees, Opportunity Knocks: Organic Chemistry for Fragment-Based Drug Discovery (FBDD). *Angew. Chemie Int. Ed*. 55 (2016) 488–492. https://doi.org/10.1002/anie.201506783.

[17] C. Temperini, A. Innocenti, A. Mastrolorenzo, A. Scozzafava, C.T. Supuran, Carbonic anhydrase inhibitors. Interaction of the antiepileptic drug sulthiame with twelve mammalian isoforms: Kinetic and X-ray crystallographic studies. *Bioorg. Med. Chem. Lett.* 17 (2007) 4866–4872. https://doi.org/10.1016/j.bmcl.2007.06.044.

[18] O. Akgul, A. Angeli, S. Selleri, C. Capasso, C.T. Supuran, F. Carta, Taurultams incorporating arylsulfonamide: First in vitro inhibition studies of α-, β- and γ-class Carbonic Anhydrases from Vibrio cholerae and Burkholderia pseudomallei. *Eur. J. Med. Chem*. 219 (2021) 113444. https://doi.org/10.1016/j.ejmech.2021.113444.

[19] R.G. Khalifah, The carbon dioxide hydration activity of carbonic anhydrase. I. Stop-flow kinetic studies on the native human isoenzymes B and C. *J. Biol. Chem.* 246 (1971) 2561. http://www.ncbi.nlm.nih.gov/pubmed/4994926 (erişim 26 Ağustos 2019).

[20] C. Temperini, A. Cecchi, A. Scozzafava, C.T. Supuran, Carbonic anhydrase inhibitors. Comparison of chlorthalidone, indapamide, trichloromethiazide, and furosemide X-ray crystal structures in adducts with isozyme II, when several water molecules make the difference. *Bioorg. Med. Chem*. 17 (2009) 1214–1221. https://doi.org/10.1016/j.bmc.2008.12.023.

[21] M. Zanda, Trifluoromethyl group: an effective xenobiotic function for peptide backbone modification. *New J. Chem*. 28 (2004) 1401. https://doi.org/10.1039/b405955g.

[22] E. Berrino, B. Michelet, A. Martin-Mingot, F. Carta, C. Supuran, S. Thibaudeau. Modulating the Efficacy of Carbonic Anhydrase Inhibitors through Fluorine Substitution. *Angew. Chemie Int. Ed*. (2021) anie.202103211. https://doi.org/10.1002/anie.202103211.

[23] https://www.rcsb.org/structure/1ZGF, (y.y.). https://doi.org/10.2210/pdb1ZGF/pdb.

[24] E.M.L. Smith, H. Pang, C. Cirrincione, S. Fleishman, E.D. Paskett, T. Ahles, L.R. Bressler, C.E. Fadul, C. Knox, N. Le-Lindqwister, P.B. Gilman, C.L. Shapiro, for the Alliance for Clinical Trials in Oncology, Effect of Duloxetine on Pain, Function, and Quality of Life Among Patients With Chemotherapy-Induced Painful Peripheral Neuropathy. *JAMA*. 309 (2013) 1359. https://doi.org/10.1001/jama.2013.2813.

[25] L. Di Cesare Mannelli, E. Lucarini, L. Micheli, I. Mosca, P. Ambrosino, M.V. Soldovieri, A. Martelli, L. Testai, M. Taglialatela, V. Calderone, C. Ghelardini, Effects of natural and synthetic isothiocyanate-based H 2 S-releasers against chemotherapy-induced neuropathic pain: Role of Kv7 potassium channels. *Neuropharmacology*. 121 (2017) 49–59. https://doi.org/10.1016/j.neuropharm.2017.04.029.

[26] Smriti Iyengar, Amy A. Webster, Susan K. Hemrick-Luecke, Jimmy Yu Xu and Rosa Maria A. Simmons. Efficacy of Duloxetine, a Potent and Balanced Serotonin-Norepinephrine Reuptake Inhibitor in Persistent Pain Models in Rats. Journal of Pharmacology and Experimental Therapeutics November 2004, 311 (2) 576-584;

[27] E. Berrino, A. Angeli, D.D. Zhdanov, A.P. Kiryukhina, A. Milaneschi, A. De Luca, M. Bozdag, S. Carradori, S. Selleri, G. Bartolucci, T.S. Peat, M. Ferraroni, C.T. Supuran, F. Carta, Azidothymidine “Clicked” into 1,2,3-Triazoles: First Report on Carbonic Anhydrase–Telomerase Dual-Hybrid Inhibitors. *J. Med. Chem*. 63 (2020) 7392–7409. https://doi.org/10.1021/acs.jmedchem.0c00636.

[28] E. Berrino, L. Milazzo, L. Micheli, D. Vullo, A. Angeli, M. Bozdag, A. Nocentini, M.

Menicatti, G. Bartolucci, L. di Cesare Mannelli, C. Ghelardini, C.T. Supuran, F. Carta, Synthesis and Evaluation of Carbonic Anhydrase Inhibitors with Carbon Monoxide Releasing Properties for the Management of Rheumatoid Arthritis. *J. Med. Chem*. 62 (2019) 7233–7249. https://doi.org/10.1021/acs.jmedchem.9b00845.

[29] O. Akgul, S. Singh, J.T. Andring, R. McKenna, S. Selleri, F. Carta, A. Angeli, C.T. Supuran, Handling drug-target selectivity: A study on ureido containing Carbonic Anhydrase inhibitors. *Eur. J. Med. Chem*. 212 (2021) 113035. https://doi.org/10.1016/j.ejmech.2020.113035.

[30] M. Buonanno, A. Di Fiore, E. Langella, K. D'Ambrosio, C. T. Supuran, S. M. Monti, G. De Simone. The Crystal Structure of a hCA VII Variant Provides Insights into the Molecular Determinants Responsible for Its Catalytic Behavior. *Int. J. Mol. Sci*. 19 (2018) 1571. doi: 10.3390/ijms19061571.

[31] Z. Otwinowsk, W. Minor. Processing of X-ray diffraction data collected in oscillation mode. *Methods Enzymol*. 276 (1997) 307-326. doi: 10.1016/S0076-6879(97)76066-X.

[32] A. T. Brunger. Version 1.2 of the Crystallography and NMR system. *Nat. Protoc*. 11 (2007) 2728-2733. doi: 10.1038/nprot.2007.406.

[33] T. A. Jones, J. Y. Zou, S. W. Cowan, M. Kjeldgaard. Improved methods for building protein models in electron density maps and the location of errors in these models. *Acta Crystallogr A*. 147 (1991) 110-119. doi: 10.1107/s0108767390010224

[34] F. H. Allen. The Cambridge Structural Database: a quarter of a million crystal structures and rising. A*cta Crystallogr B*. 58 (2002) 380-388. doi: 10.1107/s0108768102003890.

[35] R. A. Engh, R. Huber. Accurate bond and angle parameters for X-ray protein structure refinement. *Acta Cryst*. A47 (1991) 392-400. https://doi.org/10.1107/S0108767391001071.

[36] G.J. Kleywegt, K. Henrick, E.J. Dodson, D.M.F. van Aalten. Pound-wise but penny-foolish: How well do micromolecules fare in macromolecular refinement ? *Structure* 11 (2003) 1051-1059. doi: 10.1016/s0969-2126(03)00186-2.

[37] R. A. Laskowski, M. W. Macarthur, D. S. Moss, J. M. Thornton. Procheck - a Program to Check the Stereochemical Quality of Protein Structures. *J. Appl. Cryst*. 26 (1993) 283-291. https://doi.org/10.1107/S0021889892009944

[38] R. W. W. Hooft, G. Vriend, C. Sander, E. E. Abola. Errors in protein structures. *Nature* 381 (1996) 272. https://doi.org/10.1038/381272a0.

[39] J.C. McGrath, E. Lilley, Implementing guidelines on reporting research using animals (ARRIVE etc.): new requirements for publication in BJP. *Br. J. Pharmacol.* 172 (2015) 3189–3193. https://doi.org/10.1111/bph.12955.

[40] L. Micheli, L. Di Cesare Mannelli, F. Del Bello, M. Giannella, A. Piergentili, W. Quaglia, D. Carrino, A. Pacini, C. Ghelardini, The Use of the Selective Imidazoline I1 Receptor Agonist Carbophenyline as a Strategy for Neuropathic Pain Relief: Preclinical Evaluation in a Mouse Model of Oxaliplatin-Induced Neurotoxicity. *Neurotherapeutics.* 17 (2020) 1005–1015. https://doi.org/10.1007/s13311-020-00873-y.

[41] H.R. Arias, H.-S. Tae, L. Micheli, A. Yousuf, C. Ghelardini, D.J. Adams, L. Di Cesare Mannelli, Coronaridine congeners decrease neuropathic pain in mice and inhibit α9α10 nicotinic acetylcholine receptors and CaV2.2 channels. *Neuropharmacology*. 175 (2020) 108194. https://doi.org/10.1016/j.neuropharm.2020.108194.

[42] A. Pacini, L. Micheli, M. Maresca, J.J.V. Branca, J.M. McIntosh, C. Ghelardini, L. Di Cesare Mannelli, The α9α10 nicotinic receptor antagonist α-conotoxin RgIA prevents neuropathic pain induced by oxaliplatin treatment. *Exp. Neurol*. 282 (2016) 37–48. https://doi.org/10.1016/j.expneurol.2016.04.022.